Published in final edited form as:
Cell Host Microbe. 2012 March 15; 11(3): 264–276. doi:10.1016/j.chom.2012.01.018.

Autophagy Protein Rubicon Mediates Phagocytic NADPH Oxidase Activation in Response to Microbial Infection or TLR Stimulation

Chul-Su Yang[1,6], **Jong-Soo Lee**[1,2,6], **Mary Rodgers**[1], **Chan-Ki Min**[1], **June-Yong Lee**[1], **Hee Jin Kim**[1], **Kwang-Hoon Lee**[3], **Chul-Joong Kim**[2], **Byungha Oh**[3], **Ebrahim Zandi**[1], **Zhenyu Yue**[4], **Igor Kramnik**[5], **Chengyu Liang**[1], and **Jae U. Jung**[1,*]

[1]Department of Molecular Microbiology and Immunology, University of Southern California, Keck School of Medicine, Harlyne J. Norris Cancer Research Tower, 1450 Biggy Street, Los Angeles, California 90033, USA

[2]College of Veterinary Medicine, Chungnam National University, 220 Gung-Dong, Yuseong-Gu, Daejeon 305-764, Republic of Korea

[3]Department of Biological Sciences, KAIST Institute for the Biocentury, Korea Advanced Institute of Science and Technology, Daejeon, 305-701, Korea

[4]Department of Neurology, Mount Sinai School of Medicine, One Gustave L Levy Place, New York, NY 10029, USA

[5]Pulmonary Center, Department of Medicine, National Emerging Infectious Diseases Laboratory, Boston University School of Medicine, Boston, MA, 02118, USA

Summary

Phagocytosis and autophagy are two important and related arms of the host's first-line defense against microbial invasion. Rubicon is a RUN domain containing cysteine-rich protein that functions as part of a Beclin-1-Vps34-containing autophagy complex. We report that Rubicon is also an essential, positive regulator of the NADPH oxidase complex. Upon microbial infection or Toll-like-receptor 2 (TLR2) activation, Rubicon interacts with the p22*phox* subunit of the NADPH oxidase complex, facilitating its phagosomal trafficking to induce a burst of reactive oxygen species (ROS) and inflammatory cytokines. Consequently, ectopic expression or depletion of Rubicon profoundly affected ROS, inflammatory cytokine production, and subsequent antimicrobial activity. Rubicon's actions in autophagy and in the NADPH oxidase complex are functionally and genetically separable, indicating that Rubicon functions in two ancient innate immune machineries, autophagy and phagocytosis, depending on the environmental stimulus. Rubicon may thus be pivotal to generating an optimal intracellular immune response against microbial infection.

Introduction

Phagocytes play an essential role in host defenses against microbial pathogens (Flannagan et al., 2009; Huang et al., 2009; Lambeth, 2004; Sumimoto, 2008). The enzyme responsible for

*Correspondence: jaeujung@med.usc.edu.
[6]These authors contributed equally to this work

Supplemental Information: Supplemental Information includes Supplemental Experimental Procedures and seven figures and can be found with this article online doi:10.1016/j.chom.2012.01.018.

superoxide anion production and, consequently, reactive oxygen species (ROS) generation, is called the NADPH oxidase or respiratory burst oxidase. Inactive in resting macrophages and neutrophils, NADPH oxidase is activated by exposure to microorganisms or inflammatory mediators, resulting in nonmitochondrial production of ROS. The oxidase consists of the common integral membrane protein subunit, p22*phox*, and catalytic subunit gp91*phox* (NOX2), together with the regulatory subunits p47*phox*, p40*phox*, p67*phox* and the small GTPase Rac. ROS are themselves rapidly toxic and can kill microbes, but they also participate in host defense by inducing the activation of NF-κB and release of proinflammatory mediators, such as IL-1α, IL-6, MCP-1, and TNFα. The importance of NADPH oxidase in host defenses is illustrated by a life-threatening genetic disorder called chronic granulomatous disease (CGD), in which the phagocyte enzyme is dysfunctional, leading to life-threatening bacterial and fungal infections (Jones et al., 2008; Martire et al., 2008; Matute et al., 2009; van den Berg et al., 2009; Winkelstein et al., 2000).

Autophagy is an emerging host innate immune pathway that is a highly regulated homeostatic process wherein worn-out proteins, malfunctioning organelles, and invading microbes are swept up and degraded by tiny “vacuum cleaners” (Deretic and Klionsky, 2008; Deretic and Levine, 2009). Thus, autophagy is an important innate safeguard mechanism for protecting the organism against unwanted materials and guests and also for keeping the organism healthy. Specifically, the autophagic machinery functions in host defenses, called xenophagy, by degrading invading pathogens, including intracellular bacteria (e.g., *Shigella flexneri* and *Mycobacterium tuberculosis*), animal viruses (e.g., alphaviruses and herpes virus), and plant viruses (tobacco mosaic virus) (Kim et al., 2010; Orvedahl and Levine, 2009). Autophagy may protect infected cells by either enhancing degradation of intracellular pathogens to block microbial replication or by maintaining cellular nutrient status during periods of microbial parasitism.

RUN domain protein as Beclin-1 interacting and cysteine-rich containing (Rubicon) autophagy protein was recently identified as a Beclin-1-binding partner that interacts through its coiled-coil domains (Matsunaga et al., 2009; Zhong et al., 2009). Rubicon contains a RUN domain, a serine-rich-N (SR-N) region, a coiled-coil domain, a serine-rich-C (SR-C) region, and a cysteine-rich region. It localizes to the late endosome/lysosome but not the autophagosome. Knockdown of Rubicon results in a marked increase in the number of autolysosomes as well as in receptor degradation, whereas its overexpression leads to abnormal morphology of late endosome/lysosomes and the inhibition of autophagosome/endosome maturation, suggesting that Rubicon negatively regulates the maturation step of autophagy and the endocytic pathway (Matsunaga et al., 2009; Zhong et al., 2009). Furthermore, Rubicon interacts with Vps34 lipid kinase and Rab7 GTPase through its N-terminal RUN domain and C-terminal cysteine-rich domain, respectively, which ultimately controls Vps34 and Rab7 activity (Sun et al., 2010, 2011; Tabata et al., 2010).

Phagocytosis and autophagy cooperate together as part of the host's first-line of immune defense against microbial invasions (Huang et al., 2009; Sanjuan et al., 2007; Tal et al., 2009; Travassos et al., 2010). Here, we report that Rubicon autophagy protein is an essential positive regulator of the NADPH oxidase complex, inducing ROS production upon microbial infection or plasma TLR2 activation. Remarkably, Rubicon's actions in the Beclin-1-Vps34-containing autophagy complex and the p22*phox*-gp91*phox*-containing NADPH oxidase complex are functionally and genetically separable. Thus, Rubicon orchestrates two innate immune machineries, autophagy and phagocytosis, to ultimately optimize the timing and efficiency of host antimicrobicidal activity in response to specific environmental stimuli.

Results

Rubicon Interaction with the p22*phox*-gp91*phox* NADPH Oxidase Complex

Because engaging the autophagy pathway via TLR signaling enhances phagosome maturation and destruction of the engulfed microbes (Sanjuan et al., 2007), we purified the radioactively labeled Rubicon complexes from human THP-1 cells containing vector or Flag-Rubicon upon stimulation with zymosan, a TLR2 ligand (100 μg/ml), or rapamycin (2 μM). As previously reported (Matsunaga et al., 2009; Zhong et al., 2009), Rubicon (130K) was found to associate with several proteins, Vps15 (150K), Vps34 (110K), UVRAG (85K), and Beclin-1 (60K), based on their molecular weights and coimmunoprecipitation (coIP) (Figures 1A, S1A, and S1B). Besides this complex, Rubicon also interacted with two additional proteins with the molecular weights of 91K and 22K, and these interactions periodically increased at 5 and 30 min after zymosan stimulation (Figure 1A and S1B). In contrast, Rubicon interaction with the Beclin-1-containing autophagy complex was not significantly affected under zymosan-treatment conditions (Figures 1A and S1B). Conversely, rapamycin stimulation detectably increased Rubicon interactions with the Beclin-1-containing autophagy complex without affecting its interactions with the 22K and 91K proteins (Figure 1A and S1B). Yeast two-hybrid screens with the full-length, N-terminal region (aa1-470) or C-terminal region (aa471-972) of Rubicon as baits identified the p22*phox* integral membrane subunit of the NADPH oxidase complex as a major binding partner of Rubicon full-length or its C-terminal region. Furthermore, mass spectrometry analysis of the purified zymosan stimulation-induced Rubicon complexes determined that p22*phox* and gp91*phox* are the 22K and 91K proteins that associated with Rubicon (Figure S1C). CoIP showed that Rubicon interacted strongly with exogenous and endogenous p22*phox*, and this interaction was more evident upon stimulation with zymosan (Figures 1B and 1C). Binding studies with GST-Rubicon mammalian fusions and GST-p22*phox* mammalian fusions showed that Beclin-1 and p22*phox* efficiently bound the central coiled-coil domain (CCD) (aa505-557) and the C-terminal SR (aa558-625) of Rubicon, respectively, indicating that the interactions of Rubicon with Beclin-1 and p22*phox* are genetically separable (Figure 1D). Remarkably, the N-terminal ten-amino acid sequence of p22*phox* directly and specifically bound to a bacterially purified GST-Rubicon protein in vitro because its mutant, W_6AW_9A, carrying the replacements of tryptophan residues 6 and 9 with alanines, did not do so (Figure 1D). These results indicate that Rubicon directly interacts with p22*phox*-gp91*phox* complex upon stimulation by zymosan.

Differential Rubicon Interaction Stabilizes p22*phox* and gp91*phox*

To further delineate the temporal interaction profile of Rubicon, Flag-Rubicon complexes were immunopurified upon zymosan or rapamycin stimulation and immunoblotted with various antibodies. This showed that Rubicon interactions with gp91*phox* and p22*phox* periodically increased at 5 and 30 min after zymosan stimulation, whereas its interactions with Beclin-1 and UVRAG were initially reduced (1–3 min) but immediately recovered (Figures 2A and S1D). These interactions were specific because the Rubicon ΔSR mutant lost the p22*phox*-gp91*phox* interaction but retained the Beclin-1-UVRAG interaction, whereas the ΔCCD mutant lost the Beclin-1-UVRAG interaction but retained the periodic interaction with p22*phox*-gp91*phox* (Figure 2A). In contrast, rapamycin stimulation might not considerably alter Rubicon interaction with either the Beclin-1-UVRAG complex or the p22*phox*-gp91*phox* complex (Figure S2A). When the Flag-p22*phox*, Flag-gp91*phox*, or Flag-p47*phox* complex was immunopurified, Rubicon interactions with p22*phox* or gp91*phox* also peaked at 5 and 30 min after zymosan stimulation, whereas Rubicon interaction with p47*phox* was not detected (Figure S2B). Furthermore, Rubicon interactions with p22*phox* or gp91*phox* were detected with TLR2-mediated stimulation, but not intracellular soluble PMA-induced stimulation (Figure S2C). These results indicate that

although Rubicon is primarily present in the Beclin-1-UVRAG complex under normal and autophagy conditions, it is periodically recruited to the p22*phox*-gp91*phox* complex upon TLR2 activation.

In virtually all CGD patients with cytochrome b_{558} mutations, neutrophils lack both gp91*phox* and p22*phox*, suggesting that the formation of the p22*phox*-gp91*phox* heterodimer is important for the stable expression of each subunit (Jones et al., 2008; Malech and Hickstein, 2007; Martire et al., 2008; Matute et al., 2009; van den Berg et al., 2009; Winkelstein et al., 2000). We found that the expression or depletion of the Rubicon gene markedly increased or decreased, respectively, the levels of endogenous and exogenous p22*phox* and gp91*phox* expression, but not p47*phox*, in a binding-specific manner because the ΔSR mutant did not do so (Figures 2B, S2D, S2E, and S2F). Cycloheximide (CHX) treatment further confirmed that Rubicon expression significantly stabilizes p22*phox* level (Figure 2C). The nmf333 mouse strain carrying the p22*phox* $Y_{121}H$ mutation dramatically interferes with either the synthesis or stability of the p22*phox* protein (Nakano et al., 2008). Remarkably, Rubicon also bound and stabilized the p22*phox* $Y_{121}H$ mutant (Figure 2D). These findings suggest that Rubicon effectively enhances p22*phox* stability in a binding-dependent manner.

Rubicon Facilitates p22*phox* Phagosomal Localization and Phagocytosis

We next examined the effect of Rubicon on p22*phox* localization following infection with heat-killed (HK)-TRITC-labeled or live-TRITC-labeled *Listeria*(*L.*)*monocytogenes*. Rubicon expression apparently increased p22*phox* colocalization with HK or live-TRITC-*L. monocytogenes*, as well as the number of phagosomes containing HK or live-TRITC-*L. monocytogenes* (Figures 3A, S3A, S3C, and S3D). Conversely, depletion of Rubicon expression not only suppressed p22*phox* colocalization with HK or live-TRITC-*L. monocytogenes*, but also reduced phagosome numbers (Figures 3A, S3B, S3C, and S3D). Expression of Rubicon WT and ΔCCD markedly increased the numbers of HK or live-TRITC-*L. monocytogenes*-positive phagosomes, and both completely colocalized with p22*phox* (Figures 3B, S3E, S3F, S3G, S3H, S3I, S3J, and S3K). In striking contrast, not only did the Rubicon ΔSR mutant display diffuse cytosolic staining, but it also apparently prevented p22*phox* from trafficking into HK or live-TRITC-*L. monocytogenes*-positive phagosomes (Figures 3B, S3H, S3I, S3J, and S3K). Furthermore, upon time-course exposure to Texas red-labeled opsonized-zymosan particles, Rubicon WT and ΔCCD extensively colocalized with p22*phox* and gp91*phox* in the zymosan-particle-containing phagosomes, and also significantly increased the phagosome numbers (Figures 3C and S3L). In contrast, the zymosan-induced translocation of p22*phox* into phagosomes was not observed upon expression of the Rubicon ΔSR mutant (Figure 3C and S3L). Furthermore, when cells were treated with zymosan and Lysotracker or with GFP-*L. monocytogenes* infection and a self-quenched red BODIPY dye-conjugated bovine albumin serum (DQ-Red BSA), Rubicon WT and ΔCCD colocalized extensively with Lysotracker-positive compartments or DQ-Red BSA-positive and GFP-*L. monocytogenes*-containing phagosomal compartments, respectively (Figures S3M and S3N).

Previous studies have found that the Vps34 is responsible for phosphatidylinositol 3-phosphate (PtdIns-3-P) synthesis and essential for phagolysosome formation (Vieira et al., 2001), and that it is also targeted and inhibited by Rubicon (Sun et al., 2010, 2011; Tabata et al., 2010). To examine the effect of Rubicon on phagosomal maturation upon zymosan stimulation, we measured Vps34 activity using the p40(phox) PX–EGFP fusion protein (Liang et al., 2008). Under normal conditions, p40(phox) PX–EGFP was visible in Raw264.7-vector cells as a few punctate structures reflecting the PtdIns-3-P-rich vesicles, whereas the punctate numbers of p40(phox) PX–EGFP were detectably low in Rubicon WT-, ΔCCD-, or ΔSR-expressing Raw264.7 cells (Figure S3O). By striking contrast, the

intensity and number of p40(phox) PX–EGFP–stained vesicles increased dramatically in vector-, Rubicon WT-, ΔCCD-, or ΔSR-expressing Raw264.7 cells upon zymosan treatment at similar levels (Figure S3O). These results indicate that although Rubicon WT, ΔCCD, and ΔSR suppress Vps34 activity under normal conditions, they show little or no suppressive effects on Vps34 activity under zymosan-treatment conditions. Finally, the levels of internalized GFP-*L. monocytogenes* increased by nearly 3- to 4-fold upon Rubicon WT and ΔCCD mutant expression, but decreased 3- to 4-fold upon ΔSR mutant expression (Figure S4A).

To further delineate Rubicon's actions in the phagosomal trafficking of the p22*phox*-gp91*phox*-containing NADPH complex, Raw246.7 cells were infected with Rubicon-overexpressing or Rubicon-specific shRNA-mediated knockdown adenoviruses or p22*phox*-specific or gp91*phox*-specific shRNA-mediated knockdown lentiviruses and then stimulated with zymosan-coated or IgG-coated beads for various times. The latex bead-containing phagosome fractions were subsequently purified by sucrose-step-gradient-ultracentrifugations. Under normal conditions, Rubicon-p22*phox*-gp91*phox* was recruited to phagosomes at kinetics similar to Beclin-1-UVRAG-Vps34. Under Rubicon-overexpression conditions, Rubicon-p22*phox*-gp91*phox* was recruited to phagosomes earlier (5 min of stimulation) than Beclin-1-UVRAG-Vps34 (15 min). In contrast, under Rubicon-depletion conditions, the phagosomal recruitment of Rubicon-p22*phox*-gp91*phox* was delayed and dramatically reduced, whereas the phagosomal recruitment of Beclin-1-UVRAG-Vps34 was not affected (Figure 3D). Additionally, the expression levels of Rubicon, p22*phox*, and gp91*phox* were directly correlated with their phagosomal recruitment levels, whereas p47*phox* was independently recruited to phagosomes (Figure S4B). Finally, Rubicon's effects were TLR2-signaling specific because they were not detected upon IgG stimulation (Figure S4C). These results collectively indicate that Rubicon facilitates the phagosomal trafficking of the p22*phox*-gp91*phox* complex in a binding-dependent manner, and that the Rubicon-p22*phox*-gp91*phox* complex and the Beclin-1-UVRAG-Vps34 complex are independently recruited to phagosomes.

Rubicon Activates NADPH Oxidase Activity in a p22*phox*-Binding-Dependent Manner

We next used the oxidative fluorescent dyes dihydroethidium (DHE) and 5,6-chloromethyl-2′,7′-dichlorodihydrofluorescein diacetate acetyl ester (CM-H_2DCFDA) to detect O_2^- and H_2O_2 production, respectively (Yang et al., 2009). Upon zymosan stimulation, the fluorescent signal intensities attributed to O_2^- and H_2O_2 production increased profoundly in Rubicon-expressing Raw264.7 and primary mouse bone marrow-derived macrophage cells (BMDMs) compared to control cells (Figures 4A and 4B). In contrast, the antioxidant N-acetyl-L-cysteine (NAC) and the NADPH oxidase inhibitor diphenyliodonium chloride (DPI) significantly attenuated Rubicon-induced O_2^- and H_2O_2 production, respectively (Figures 4A and 4B). Additionally, Rubicon expression dramatically enhanced NADPH oxidase activity in Raw264.7 and mouse BMDMs upon stimulation with zymosan or bacterial lipoprotein (BLP), or upon infection with *L. monocytogenes* (Figures 4C and 4D). The stimulatory effect of Rubicon on NADPH consumption and phagocytosis was nearly abolished by pretreatment with the NADPH oxidase inhibitors DPI and 4-(2-aminoethyl) benzene-sulphonyl fluoride (AEBSF) (Figures 4D and S4D). By contrast, no significant difference in the PMA, LPS-, hot-alkali-depleted zymosan- or NOD2-recognizing muramyl dipeptide (MDP)-mediated release of ROS was detected between vector- and Rubicon-expressing Raw264.7 cells (Figure S4E). Furthermore, Rubicon expression increased TLR2 interaction with p22*phox*-gp91*phox* and its trafficking into zymosan-coated bead-containing phagosomes where Rubicon was also localized (Figures S5A and S5B). This action was specific because there was little or no effect on the TLR2-MyD88 interaction as well as MyD88 Y_{257} phosphorylation (Figure

S5A) (Laird et al., 2009). When A549 epithelial cells endogenously expressing NOX4 but not gp91*phox* (NOX2) were subjected to stimulation with BLP (TLR2 ligand) or LPS (TLR4 ligand), Rubicon interacted with the p22*phox*-NOX4-TLR4 complex as previously shown (Park et al., 2004) and efficiently enhanced LPS-induced NOX4 activity but showed no effect on BLP-induced signaling activities (Figures S5C, S5D, and S5E), suggesting that Rubicon targets p22*phox*, a common subunit of NOX family, and thereby affects various TLR-NOX pathways. Finally, expression of the Rubicon WT and ΔCCD, but not the ΔSR mutant, detectably enhanced phosphorylation of p38 and IκB, degradation of IκB, and nuclear localization of the NF-κB p65 subunit in Raw246.7 cells upon zymosan treatment; however, there was no significant effect on the phosphorylation of p42/44 MAPK and JNK (Figure 4E).

Rubicon's Effect on ROS, Cytokine Production and Antimicrobial Activity

NADPH oxidase signaling is known to regulate proinflammatory cytokine expression (Fang, 2004). Rubicon expressing Raw264.7 cells produced markedly higher amounts of TNF-α and IL-6 than vector-containing control cells (Figure 4F). Furthermore, lentivirus-mediated expression of Rubicon in primary mouse BMDMs led to significant increases in TNF-α and IL-6 production, whereas pretreatment with the inhibitors DPI and AEBSF nearly abolished this stimulatory effect of Rubicon on cytokine production (Figure 4F). No significant difference in the LPS-mediated activation of cytokine production was detected under Rubicon-depletion or -overexpression conditions (data not shown). Finally, the viability and growth rate of intracellular *L. monocytogenes* and *M. bovis* BCG decreased drastically in Rubicon-expressing Raw246.7, THP-1, and mouse BMDM cells compared to vector-containing control cells (Figure 4G). Consistently, the shRNA-mediated reduction of endogenous Rubicon expression led to significant attenuation of NADPH oxidase activity, ROS production, and proinflammatory cytokine production (Figures 5A, 5B, and 5C) and, thereby, to a marked reduction of bacterial killing activity against intracellular *L. monocytogenes* and *M. bovis* BCG in Raw246.7 and BMDM cells (Figure 5D).

Besides NADPH phagocyte oxidase pathways, IFN-γ-inducible nitric oxide synthase (iNOS) pathways, which generate nitric oxide (NO) radicals, represent another important antimicrobial system in phagocytic cells (Fang, 2004). To compare Rubicon's effect on the TLR2 pathway versus the IFN-γ-iNOS pathway for microbial killing activity, Raw264.7 cells were stimulated with IFN-γ, zymosan, *L. monocytogenes* infection or in combination. Rubicon expression led to only minimal differences in ROS and NO production upon IFN-γ stimulation (Figures S5F and S5G). By contrast, *L. monocytogenes* infection or zymosan stimulation produced significantly higher levels of ROS and NO production in Rubicon-expressing cells than in vector-containing cells (Figures S5F and S5G). The combination of IFN-γ stimulation and *L. monocytogenes* infection or IFN-γ stimulation and zymosan produced even higher levels of ROS and NO production in Raw246.7-Rubicon cells than in Raw246.7-vector cells (Figures S5F and S5G). In addition, the levels of antimicrobial activity correlated directly with ROS and NO production (Figure S5H). These results indicate that Rubicon is primarily involved in TLR2-mediated antimicrobial activity.

Rubicon Gene Expression Affects Mice Mortality after *L. monocytogenes* Infection

To assess whether the depletion or expression of Rubicon affects in vivo host responses to infection with *L. monocytogenes*, recombinant adenoviruses, Ad-vector, Ad-shRubicon, and Ad-Rubicon, were injected intravenously via the tail vein at a dose of ~1×10^{13} pfu/mouse twice; at 1 day postinfection, mice were challenged intraperitoneally with a lethal bacterial dose (1×10^7 CFU per mouse, n = 23 mice per each group) (Figures S6A and S6B). Mice infected with Ad-vector showed a median survival of 6 days; mice infected with Ad-shRubicon died detectably sooner (median survival, 4 days), and mice infected with Ad-

Rubicon showed a significantly delayed mortality rate (median survival, 8 days) and an increased survival rate (40% survival) (Figure 6A). To determine whether these effects were due to impaired or enhanced bacterial clearance in the Rubicon-depleted or Rubicon-expressing mice, respectively, we measured the bacterial loads, serum cytokine levels, and Rubicon expressions in the liver and spleen at 5 days after infection with a lower bacterial dose (1×10^6 CFU per mouse). Under these conditions, Rubicon-depleted mice or Rubicon-expressing mice had ~1,000-fold higher or ~10- to 100-fold lower bacterial loads in both organs, respectively, compared to mice infected with Ad-vector (Figure 6B). Correlated with the bacterial loads, the serum levels of TNF-α and IL-6 and the NADPH oxidase activity in splenocytes were lower in Rubicon-depleted mice and higher in Rubicon-expressing mice than in mice infected with Ad-vector (Figures 6C and 6D).

To further investigate Rubicon's effect on in vivo host responses to *L. monocytogenes* infection, we generated double-SRA-rtTA/Flag-Rubicon transgenic mice that carry both reverse tetracycline transactivator (rtTA) under the control of macrophage-specific promoter, a modified human scavenger receptor A (SRA) promoter (Pan et al., 2008), and Flag-tagged Rubicon under the control of tetracycline-inducible promoter. Immunoblot and confocal microscopy analyses of splenocytes isolated from transgenic SRA-rtTA/Flag-Rubicon mice showed the doxycycline-inducible, macrophage-specific expression of Rubicon (Figures S6C and S6D). At 7 days post-treatment with doxycycline, mice were subsequently challenged intravenously with a lethal *L. monocytogenes* dose (1×10^7 CFU per mouse, n = 6 mice per each group). Untreated SRA-rtTA/Flag-Rubicon mice showed a median survival of ~6 days, but doxycycline-treated mice showed 60% survival rate (Figure 6E). In addition, untreated mice had ~100- to 300-fold higher *L. monocytogenes* loads in spleen and liver, respectively, compared to doxycycline-treated mice (Figure 6F). Correlated with the *L. monocytogenes* loads, untreated mice showed much lower serum TNF-α and IL-6 levels and less severe infection-induced splenomegaly and inflammation than doxycycline-treated mice (Figures 6G, 6H, and S6E). These results unambiguously show that host defenses against bacterial infection are substantially affected by the levels of Rubicon expression.

Rubicon Plays Distinctive Roles in Conventional and TLR-Signaling-Mediated Autophagy

To further delineate Rubicon's actions in the autophagy complex and the NADPH complex, Raw264.7 cells expressing Rubicon mutants were evaluated for their phagocytosis and autophagy activities in comparison to those of cells expressing WT. The ΔCCD mutant induced NADPH oxidase activity, ROS production, proinflammatory cytokine production, and bacterial killing activity as strongly as WT, whereas the expression of the ΔSR or ΔCDD/SR mutants showed suppressive or no effects under the same conditions (Figures 7A, 7B, and 7C). Expression of the Rubicon WT or the ΔSR mutant, both capable of binding Beclin-1, showed increased LC3-II and p62 protein levels upon rapamycin treatment or starvation, indicating suppression of autophagosome maturation step (Figure 7D). In contrast, expression of the ΔCCD mutant, which lost its ability to bind Beclin-1, showed no effect on autophagosome maturation, as evidenced by similar levels of LC3-II and p62 protein compared to vector control cells (Figure 7D). Contrastingly, Rubicon WT and its mutants showed no suppressive effect on autophagosome maturation with zymosan or BLP treatment or *L. monocytogenes* infection, likely due to the dissociation of Rubicon from the Beclin-1-UVRAG-containing autophagy complex upon such treatments (Figure 7D). Consistently, Rubicon expression specifically affected the levels of rapamycin- but not zymosan-induced p62 degradation; treatment with 3-methyladenine or bafilomycin further enhanced Rubicon-mediated suppression of the autophagosome maturation step (Figure S7). These results indicate that Rubicon plays distinctive roles in conventional and TLR-signaling-mediated autophagy, and that Rubicon's actions in the Beclin-1-UVRAG-

containing autophagy complex and in the p22*phox*-gp91*phox*-containing NADPH complex are functionally and genetically separable.

Discussion

Phagocytes play an essential role in host defenses against microbial pathogens (Flannagan et al., 2009; Huang et al., 2009; Lambeth, 2004; Sumimoto, 2008). Additionally, autophagy-mediated cytoprotective mechanisms sequester invading pathogens for degradation. Here, we report that Rubicon autophagy protein functions as a positive regulator of the phagocytic NADPH oxidase complex to induce a ROS burst, inflammatory cytokine production, and, thereby, potent antimicrobial activities.

Rubicon Interaction Induces the Stability of p22*phox* and gp91*phox*

Expression or depletion of the Rubicon gene markedly increased or decreased, respectively, the levels of endogenous and exogenous p22*phox* and gp91*phox* expression in a binding-specific manner. The p22*phox* $Y_{121}H$ substitution mutation discovered in p22*phox*-deficient nmf333 mice does not diminish its mRNA expression but interferes with either its protein synthesis or stability (Nakano et al., 2008). Rubicon interaction also increased the stability of this p22*phox* $Y_{121}H$ mutant. Rubicon interaction may facilitate the protein folding and/or tight complex formation of p22*phox*-gp91*phox*. It should also be noted that, because p22*phox* is a common subunit of the NADPH oxidase (NOX) family (Lambeth, 2004), Rubicon's effect should not be limited to the gp91*phox* (NOX2)-TLR2 pathway but likely extends to various other NOX members. Rubicon plays a primary role in the gp91*phox*-TLR2 pathway in THP-1, RAW264.7, and BMDM cells where gp91*phox*, but not NOX4, is expressed. Conversely, when human lung epithelial cells and umbilical vascular endothelial cells expressing NOX4 but not gp91*phox* were subjected to BLP or LPS stimulation, Rubicon interacted with the p22*phox*-NOX4 complex. This interaction efficiently increased LPS-induced NADPH oxidase but not BLP-induced NADPH oxidase activity (Figures S5A, S5B, S5C, S5D, and S5E and unpublished results), indicating that Rubicon targets p22*phox*, a common subunit of the NOX family and, hence, affects various NOX pathways, depending on its expression profiles (Bedard and Krause, 2007).

Rubicon Interactions with Beclin-1 Autophagy Complex and NADPH Oxidase Complex

Previous studies showed that TLR signaling usurps autophagy components to increase the efficiency of phagocytosis, thereby providing a potential link between these two ancient microbial defense mechanisms (Huang et al., 2009; Sanjuan et al., 2007; Tal et al., 2009). We demonstrate that the stimulus-dependent interactions of Rubicon with the Beclin-1-UVRAG-Vps34 autophagy complex and the NADPH oxidase complex appear to be an important event for crosstalk between these two innate immune machineries: Although Rubicon associates with the Beclin-1-UVRAG-Vps34 containing autophagy complex under normal conditions, it periodically interacts with p22*phox* of the NADPH oxidase complex upon TLR activation. In contrast, rapamycin stimulation might not considerably affect Rubicon interaction with either the Beclin-1-UVRAG-Vps34 autophagy complex or the p22*phox*-gp91*phox* NADPH oxidase complex. Consistently, the Rubicon-p22*phox*-gp91*phox* complex and the Beclin-1-UVRAG-Vps34 complex are independently recruited to phagosomes upon TLR simulation, with Rubicon-p22*phox*-gp91*phox* recruited to phagosomes earlier (5 min of stimulation) than Beclin-1-UVRAG-Vps34 (15 min). Therefore, the obvious question is: what types of molecular mechanisms specifically determine Rubicon's interactions with the Beclin-1-UVRAG-Vps34 autophagy complex or with the p22*phox*-gp91*phox* NADPH oxidase complex? The fact that the C-terminal SR region of Rubicon is sufficient for binding p22*phox* suggests that TLR-mediated signaling may trigger rapid structural alterations or modifications of the Rubicon C-terminal SR

region, leading to its association with the p22*phox*-gp91*phox* complex. Detailed biochemical studies will be necessary to provide evidence for or against this hypothesis.

Rubicon-Mediated Increase of Phagosome Trafficking of p22*phox*-g91*phox* Complex

We showed that Rubicon efficiently facilitates the phagosomal trafficking of the p22*phox*-gp91*phox* complex in a binding-dependent manner. Recent studies have shown that Rubicon interacts with the Rab7 GTPase protein through its C-terminal cysteine-rich domain (Sun et al., 2010). Because Rab7 regulates membrane trafficking by cycling between inactive (i.e., GDP-bound) and active (i.e., GTP-bound) states, the Rubicon-Rab7 interaction is likely involved in facilitating the phagosome recruitment of the p22*phox*-gp91*phox* complex. Besides increasing p22*phox*-gp91*phox* phagosome recruitment, Rubicon expression considerably enhanced phagocytosis, an event requiring the coordination of multiple processes, including TLR2 signaling, phagocytic uptake, and phagosomal formation/maturation. A previous study (Yang et al., 2009) showed that gp91*phox* associates with TLR2 in response to ligand stimulation or microbial infection and that this association is required for efficient phagocytosis, ROS burst, and inflammatory cytokine production in macrophages. In line with this, we showed that Rubicon not only markedly enhanced p22*phox*-gp91*phox* stability, resulting in increased p22*phox*-gp91*phox* interaction with TLR2, but also robustly increased the recruitment of TLR2 to phagosomes where Rubicon, p22*phox*, and gp91*phox* colocalized. Furthermore, these effects were completely abrogated by treatment with the NADPH oxidase inhibitors, DPI or AEBSF, indicating the important role of NADPH oxidase activity for phagocytosis. Thus, Rubicon may affect various steps of the tightly interrelated phagocytic processes, including the TLR signaling pathway and phagosome trafficking. It should be also noted that besides NADPH phagocyte oxidase pathways, IFN-γ-inducible iNOS pathways generating NO radicals represent another important antimicrobial system in phagocytic cells (Fang, 2004). Particularly, a recent study reported that, similar to Rubicon, a family of IFN-γ-inducible guanylate-binding protein (Gbp) (Kim et al., 2011) restricts Listeria infection by recruiting gp91*phox*-p22*phox* NADPH oxidase complex and autophagy effectors (Atg4b and p62/Sqstm1) to the bacteria-containing autophagolysosomes. Although Rubicon expression contributed to only minimal differences in ROS and NO production upon IFN-γ stimulation, further study is necessary to define the molecular roles of Rubicon in NADPH phagocyte oxidase-mediated and IFN-γ-inducible iNOS-mediated antimicrobial pathways. Nevertheless, these indicate that phagocytosis-mediated and xenophagy-mediated microbicidal activity induced by signaling molecules suchas Rubicon and Gbp may ultimately provide host protection against a broad spectrum of pathogens.

Rubicon Functions in Autophagy and Phagocytosis

Autophagy and phagocytosis have been shown to efficiently collaborate to generate effective host responses against microbial infections as part of host's initial innate immunity (Deretic, 2011; Kim et al., 2010; Kumar and Rao, 2011; Levine et al., 2011). Based on previous and current studies, we hypothesize that, due to its ability to bind the Beclin-1-UVRAG-Vps34 autophagy complex and the p22*phox*-gp91*phox* NADPH complex in a genetically separable manner, Rubicon targets two ancient innate immune machineries, autophagy and phagocytosis, to efficiently orchestrate intracellular antimicrobial responses. Under normal conditions, Rubicon first functions as a gatekeeper of autophagy by interacting with the Beclin-1-UVRAG-Vps34 complex to suppress the autophagy and endocytic maturation step (Matsunagaetal., 2009; Zhongetal., 2009). Upon TLR stimulation, however, Rubicon interacts with the NADPH oxidase phagocytic complex, resulting in two potential events in a timely and efficient fashion: 1) the stabilization and phagosomal recruitment of the *p22phox-gp91phox* complex, thereby activating NADPH oxidase activity to induce ROS-mediated oxidative microbicidal activity; and 2) the release of Beclin-1-

UVRAG-Vps34 lipid kinase complex from its suppression mode, allowing it to move to phagosomes and ultimately induce phagosomal maturation as a nonoxidative cytoprotective antimicrobial activity. Furthermore, we have demonstrated in an accompanying paper that Rubicon acts as a physiological brake for CARD9-mediated immune responses in a stimulation-specific manner (Yang et al., 2012 [accompanying paper, this issue of *Cell Host & Microbe*]). These indicate that Rubicon is a multifaceted immune modulatory protein that regulates host innate immune response. Future studies will be directed to understanding how Rubicon coordinates various innate resistance machineries to generate an optimal intracellular immune milieu for controlling microbial infection.

Experimental Procedures

Measurement of Intracellular ROS and Determination of NADPH Oxidase Activity

The oxidative fluorescent dyes DHE (1 μM) and CM-H_2DCFDA (2 μM) were used to detect O_2^- and H_2O_2 production, respectively, using confocal microscopy and lucigenin (*bis-N*-methylacridinium nitrate, 5×10^{-6} M) chemiluminescence assays to measure NADPH oxidase (Yang et al., 2009). The values are expressed as relative light units per 1×10^5 cells.

Phagocytosis Assays

In brief, *L. monocytogenes* was fluorescently labeled with tetramethylrhodamine isothiocyanate (TRITC; Sigma) in 0.1 M carbonate (pH 9.5) and stored at 4°C. TRITC-labeled *L. monocytogenes* or GFP-*L. monocytogenes* (10^8 CFU) were then used to infect cells in a 12-well plate for indicated times at 37°C. Partially attached, noningested bacteria were removed by 1 hr of treatment with 50 μg/ml gentamycin, using trypan blue as a quenching agent to exclude fluorescence from the cell surface. Samples were then fixed with 4% p-formaldehyde and analyzed using a laser-scanning confocal microscopy (Nikon Eclipse C1) or BD FACSCanto II (Becton Dickinson; minimum 10,000 cells per sample) to identify the proportion of cells associated with fluorescent bacteria, used as a marker for phagocytosis.

Zymosan or TRITC-labeled opsonized-zymosan particles (Molecular Probes) were fed to cells for indicated time periods, with brief centrifugation upon zymosan addition to ensure particle contact with the cells. Cells were lifted in PBS containing 1 mM EDTA, 1 mM sodium azide, and 2.4 U/ml proteinase K (to remove bound but not internalized zymosan particles) prior to analysis by confocal microscope or flow cytometry.

Phagosome Purification

Phagosomes were formed by the internalization of latex beads in culture medium at 37°C for the indicated times. Cells were then washed in PBS on ice, disrupted in homogenization buffer (3 mM imidazole, pH 7.4, containing 8.55% [w/w] sucrose, 2 mM phenylmethylsulfonyl fluoride, 1 μg/ml chymostatin, 1 μg/ml E-64, 1 μg/ml leupeptin, 1 μg/ml pepstatin) by nitrogen cavitation for 20 min at 300 psi in a bomb (Parr Instrument) at 4°C. After centrifugation at 1,500 rpm for 7 min to remove nuclei and unbroken cells, the supernatants containing the latex bead-containing phagosomal compartments (LBC) were subjected to stepwise sucrose gradient centrifugation. Centrifugation was carried out at 24,000 rpm for 1 hr in a SW41 Beckman swinging rotor. The LBC fractions were collected from the 10%/25% sucrose interface. The collected LBC fractions were washed with PBS. The purity of the final LBC fractions was evaluated by electron microscopy.

Quantification of *L. monocytogenes* or *M. bovis* BCG Intracellular Growth

To ensure the reliable quantification of intracellular bacteria, colony-forming unit (CFU) was utilized. Cells were infected for 1 hr with *L. monocytogenes* or for 2 hr with *M. bovis* BCG at different MOIs and washed three times with PBS, followed by incubation with a medium containing gentamycin (50 μg/ml for *L. monocytogenes)* or amikacin (200 μg/ml, *M. bovis* BCG) for 1 hr. Fresh medium containing gentamycin (5 μg/ml) or amikacin (20 μg/ml) was then used for time-course incubation. Finally, cells were harvested and lysed with 0.3% saponin (Sigma-Aldrich) to release the intracellular bacteria, and cell lysates were then resuspended vigorously, transferred to screw cap tubes, and sonicated in a preheated 37°C water bath sonicator (Elma) for 5 min. Aliquots of the sonicates were then diluted 10-fold in BHI broth (for *L. monocytogenes)* or 7H9 medium (for *M. bovis* BCG). Four dilutions of each sample were plated separately on BHI agar (for *L. monocytogenes)* or 7H10 agar (for *M. bovis* BCG) plates and incubated at 37°C with for 1 day (for *L. monocytogenes)* or 2–3 weeks (for *M. bovis* BCG).

Mice and Adenovirus Injection

Six-week-old female C57BL/6 mice were purchased from Charles River Laboratories. All animals received care in compliance with the guidelines outlined in the *Guide for the Care and Use of Laboratory Animals*. Recombinant adenoviruses were thawed immediately before injection at 25°C and diluted with saline solution to a final volume of 100 μl per mouse. Mice were held down within a restrainer and their tails were mildly heated with a heating lamp to achieve vasodilatation. Adenoviruses were injected through the tail vein slowly with a 30-gauge needle. After injection, mild pressure was applied at the spot of injection until no bleeding was achieved to prevent the backflow of virus solution. For measurement of the bacterial burdens in liver and spleen, mice were killed on day 5 after inoculation, organs were homogenized in PBS, and serial dilutions of the homogenates were plated on BHI agar plates, with colonies counted 24 hr later.

Rubicon/SRA-rtTA Mice

A transgenic mouse strain C3H.TgN(SRA-rtTA) expresses reverse tetracycline transactivator (rtTA) under the control of macrophage-specific promoter, a modified human scavenger receptor A (SRA) promoter. To make a Rubicon transgene construct, Flag-tagged Rubicon was cloned into pTRE-Tight (Clontech) between the *Afl*II and *Xba*I sites. Recombinant pTRE-Flag-Rubicon DNA was purified from agarose gel and introduced into fertilized C57BL/6 oocytes by pronuclear injection. Offspring were genotyped by PCR with specific primers. Transgene-bearing founder mice were backcrossed to the C57BL/6 mice. Transcription of the Rubicon transgene was confirmed by RT-PCR. Homozygote transgenic mice were generated by intercrossing transgene-positive animals and selecting for the transgene homozygotes, using PCR analysis. Transgene expression was induced in compound heterozygous animals and their littermates by replacing normal drinking water with 5% sucrose water containing 0.2 g/l doxycycline. Doxycyline-treated water was changed every 2 days. After 7 days of doxycycline treatment, mice were sacrificed and tissues were analyzed for Rubicon expression.

Supplementary Material

Refer to Web version on PubMed Central for supplementary material.

Acknowledgments

This work was partly supported by CA082057, CA31363, CA115284, DE019085, AI073099, AI083025, HL110609, Hastings Foundation, and Fletcher Jones Foundation (J.U.J.).; the GRL Program (K20815000001) from

National Research Foundation of Korea (B.H.O. and J.U.J.); Basic Science Research Program through the National Research Foundation of Korea funded by the Ministry of Education, Science and Technology (2011-0014785: J.S.L., C.J.K., and J.U.J.) and CA140964, AI083841, the Wright Foundation and the Baxter Foundation (C.L.). We thank Drs. Daniel Portnoy, Yoko Nakano, Mary Dinauer, and Yi Luo for reagents and Stacy Lee for manuscript preparation. Finally, we thank all of J.J.'s lab members for their discussions.

References

Bedard K, Krause KH. The NOX family of ROS-generating NADPH oxidases: physiology and pathophysiology. Physiol Rev. 2007; 87:245–313. [PubMed: 17237347]

Deretic V. Autophagy in immunity and cell-autonomous defense against intracellular microbes. Immunol Rev. 2011; 240:92–104. [PubMed: 21349088]

Deretic V, Klionsky DJ. How cells clean house. Sci Am. 2008; 298:74–81. [PubMed: 18444328]

Deretic V, Levine B. Autophagy, immunity, and microbial adaptations. Cell Host Microbe. 2009; 5:527–549. [PubMed: 19527881]

Fang FC. Antimicrobial reactive oxygen and nitrogen species: concepts and controversies. Nat Rev Microbiol. 2004; 2:820–832. [PubMed: 15378046]

Flannagan RS, Cosío G, Grinstein S. Antimicrobial mechanisms of phagocytes and bacterial evasion strategies. Nat Rev Microbiol. 2009; 7:355–366. [PubMed: 19369951]

Huang J, Canadien V, Lam GY, Steinberg BE, Dinauer MC, Magalhaes MA, Glogauer M, Grinstein S, Brumell JH. Activation of antibacterial autophagy by NADPH oxidases. Proc Natl Acad Sci USA. 2009; 106:6226–6231. [PubMed: 19339495]

Jones LB, McGrogan P, Flood TJ, Gennery AR, Morton L, Thrasher A, Goldblatt D, Parker L, Cant AJ. Special article: chronic granulomatous disease in the United Kingdom and Ireland: a comprehensive national patient-based registry. Clin Exp Immunol. 2008; 152:211–218. [PubMed: 18410635]

Kim HJ, Lee S, Jung JU. When autophagy meets viruses: a double-edged sword with functions in defense and offense. Semin Immunopathol. 2010; 32:323–341. [PubMed: 20865416]

Kim BH, Shenoy AR, Kumar P, Das R, Tiwari S, MacMicking JD. A family of IFN-gamma-inducible 65-kD GTPases protects against bacterial infection. Science. 2011; 332:717–721. [PubMed: 21551061]

Kumar D, Rao KV. Regulation between survival, persistence, and elimination of intracellular mycobacteria: a nested equilibrium of delicate balances. Microbes Infect. 2011; 13:121–133. [PubMed: 20971210]

Laird MH, Rhee SH, Perkins DJ, Medvedev AE, Piao W, Fenton MJ, Vogel SN. TLR4/MyD88/PI3K interactions regulate TLR4 signaling. J Leukoc Biol. 2009; 85:966–977. [PubMed: 19289601]

Lambeth JD. NOX enzymes and the biology of reactive oxygen. Nat Rev Immunol. 2004; 4:181–189. [PubMed: 15039755]

Levine B, Mizushima N, Virgin HW. Autophagy in immunity and inflammation. Nature. 2011; 469:323–335. [PubMed: 21248839]

Liang C, Lee JS, Inn KS, Gack MU, Li Q, Roberts EA, Vergne I, Deretic V, Feng P, Akazawa C, Jung JU. Beclin1-binding UVRAG targets the class C Vps complex to coordinate autophagosome maturation and endocytic trafficking. Nat Cell Biol. 2008; 10:776–787. [PubMed: 18552835]

Malech HL, Hickstein DD. Genetics, biology and clinical management of myeloid cell primary immune deficiencies: chronic granulomatous disease and leukocyte adhesion deficiency. Curr Opin Hematol. 2007; 14:29–36. [PubMed: 17133097]

Martire B, Rondelli R, Soresina A, Pignata C, Broccoletti T, Finocchi A, Rossi P, Gattorno M, Rabusin M, Azzari C, et al. IPINET. Clinical features, long-term follow-up and outcome of a large cohort of patients with Chronic Granulomatous Disease: an Italian multicenter study. Clin Immunol. 2008; 126:155–164. [PubMed: 18037347]

Matsunaga K, Saitoh T, Tabata K, Omori H, Satoh T, Kurotori N, Maejima I, Shirahama-Noda K, Ichimura T, Isobe T, et al. Two Beclin 1-binding proteins, Atg14L and Rubicon, reciprocally regulate autophagy at different stages. Nat Cell Biol. 2009; 11:385–396. [PubMed: 19270696]

Matute JD, Arias AA, Wright NA, Wrobel I, Waterhouse CC, Li XJ, Marchal CC, Stull ND, Lewis DB, Steele M, et al. A new genetic subgroup of chronic granulomatous disease with autosomal

recessive mutations in p40 phox and selective defects in neutrophil NADPH oxidase activity. Blood. 2009; 114:3309–3315. [PubMed: 19692703]

Nakano Y, Longo-Guess CM, Bergstrom DE, Nauseef WM, Jones SM, Bánfi B. Mutation of the Cyba gene encoding p22phox causes vestibular and immune defects in mice. J Clin Invest. 2008; 118:1176–1185. [PubMed: 18292807]

Orvedahl A, Levine B. Autophagy in Mammalian antiviral immunity. Curr Top Microbiol Immunol. 2009; 335:267–285. [PubMed: 19802570]

Pan H, Mostoslavsky G, Eruslanov E, Kotton DN, Kramnik I. Dual-promoter lentiviral system allows inducible expression of noxious proteins in macrophages. J Immunol Methods. 2008; 329:31–44. [PubMed: 17967462]

Park HS, Jung HY, Park EY, Kim J, Lee WJ, Bae YS. Cutting edge: direct interaction of TLR4 with NAD(P)H oxidase 4 isozyme is essential for lipopolysaccharide-induced production of reactive oxygen species and activation of NF-kappa B. J Immunol. 2004; 173:3589–3593. [PubMed: 15356101]

Sanjuan MA, Dillon CP, Tait SW, Moshiach S, Dorsey F, Connell S, Komatsu M, Tanaka K, Cleveland JL, Withoff S, Green DR. Toll-like receptor signalling in macrophages links the autophagy pathway to phagocytosis. Nature. 2007; 450:1253–1257. [PubMed: 18097414]

Sumimoto H. Structure, regulation and evolution of Nox-family NADPH oxidases that produce reactive oxygen species. FEBS J. 2008; 275:3249–3277. [PubMed: 18513324]

Sun Q, Westphal W, Wong KN, Tan I, Zhong Q. Rubicon controls endosome maturation as a Rab7 effector. Proc Natl Acad Sci USA. 2010; 107:19338–19343. [PubMed: 20974968]

Sun Q, Zhang J, Fan W, Wong KN, Ding X, Chen S, Zhong Q. The RUN domain of rubicon is important for hVps34 binding, lipid kinase inhibition, and autophagy suppression. J Biol Chem. 2011; 286:185–191. [PubMed: 21062745]

Tabata K, Matsunaga K, Sakane A, Sasaki T, Noda T, Yoshimori T. Rubicon and PLEKHM1 negatively regulate the endocytic/autophagic pathway via a novel Rab7-binding domain. Mol Biol Cell. 2010; 21:4162–4172. [PubMed: 20943950]

Tal MC, Sasai M, Lee HK, Yordy B, Shadel GS, Iwasaki A. Absence of autophagy results in reactive oxygen species-dependent amplification of RLR signaling. Proc Natl Acad Sci USA. 2009; 106:2770–2775. [PubMed: 19196953]

Travassos LH, Carneiro LA, Ramjeet M, Hussey S, Kim YG, Magalhães JG, Yuan L, Soares F, Chea E, Le Bourhis L, et al. Nod1 and Nod2 direct autophagy by recruiting ATG16L1 to the plasma membrane at the site of bacterial entry. Nat Immunol. 2010; 11:55–62. [PubMed: 19898471]

van den Berg JM, van Koppen E, Ahlin A, Belohradsky BH, Bernatowska E, Corbeel L, Español T, Fischer A, Kurenko-Deptuch M, Mouy R, et al. Chronic granulomatous disease: the European experience. PLoS ONE. 2009; 4:e5234. [PubMed: 19381301]

Vieira OV, Botelho RJ, Rameh L, Brachmann SM, Matsuo T, Davidson HW, Schreiber A, Backer JM, Cantley LC, Grinstein S. Distinct roles of class I and class III phosphatidylinositol 3-kinases in phago-some formation and maturation. J Cell Biol. 2001; 155:19–25. [PubMed: 11581283]

Winkelstein JA, Marino MC, Johnston RB Jr, Boyle J, Curnutte J, Gallin JI, Malech HL, Holland SM, Ochs H, Quie P, et al. Chronic granulomatous disease Report on a national registry of 368 patients. Medicine (Baltimore). 2000; 79:155–169. [PubMed: 10844935]

Yang CS, Shin DM, Kim KH, Lee ZW, Lee CH, Park SG, Bae YS, Jo EK. NADPH oxidase 2 interaction with TLR2 is required for efficient innate immune responses to mycobacteria via cathelicidin expression. J Immunol. 2009; 182:3696–3705. [PubMed: 19265148]

Yang CS, Rodgers M, Min CK, Lee JS, Kingeter L, Lee JY, Jong A, Kramnik I, Lin X, Jung JU. The autophagy regulator Rubicon is a feedback inhibitor of CARD9-mediated host innate immunity. Cell Host Microbe. 2012; 11:277–289. this issue. [PubMed: 22423967]

Zhong Y, Wang QJ, Li X, Yan Y, Backer JM, Chait BT, Heintz N, Yue Z. Distinct regulation of autophagic activity by Atg14L and Rubicon associated with Beclin 1-phosphatidylinositol-3-kinase complex. Nat Cell Biol. 2009; 11:468–476. [PubMed: 19270693]

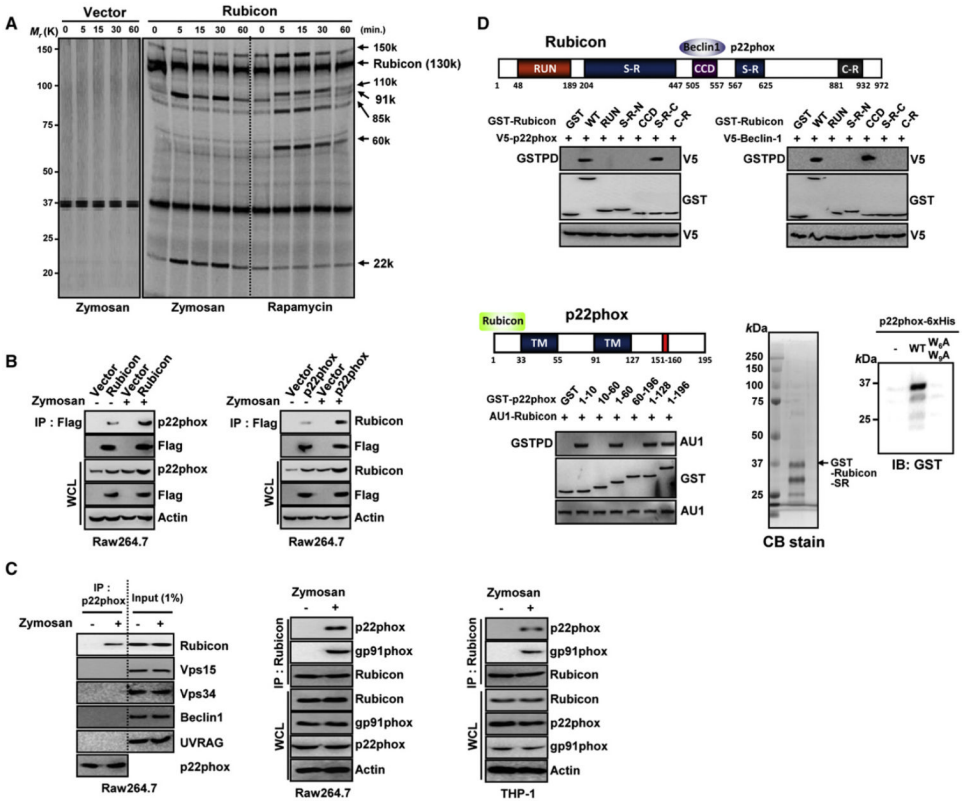

Figure 1. Rubicon Interaction with the p22*phox*-gp91*phox*NADPH Oxidase Complex

(A) Differential interactions of Rubicon with the Beclin-1-containing autophagy complex and the p22*phox*-gp91*phox* complex. Radioactively labeled THP-1 cells containing vector or Flag-Rubicon were stimulated with zymosan or rapamycin for the indicated times, followed by IP with αFlag for autoradiography.

(B) Rubicon interaction with p22*phox*. At 48 hr posttransfection with Flag-Rubicon (left) or Flag-p22*phox* (right), Raw264.7 cells were stimulated with or without zymosan for 30 min prior to immunoprecipitation (IP), followed by immunoblotting (IB).

(C) Rubicon interaction with p22phox. Raw264.7 and THP-1 cells were stimulated with zymosan for 30 min, followed by IP with αp22*phox* or αRubicon and IB.

(D) Binding mapping. Schematic diagram of Rubicon and p22*phox*. S-R, serine-rich; CCD, coiled-coil domain; C-R, cystein-rich; and TM, transmembrane (top). At 48 hr posttransfection with mammalian GST or GST-Rubicon constructs together with V5-p22*phox* (left) or V5-Beclin-1 (right) or GST or GST-p22*phox* constructs together with AU1-Rubicon (bottom left), 293T cells were used for GST pulldown, followed by IB with αV5, αGST or αAU1. (bottom right) Direct interaction between Rubicon and p22*phox*. Bacterially purified GST-RubiconSR-C was analyzed by Coomassie blue staining (left) or incubated with nickel beads alone, WT p22*phox* (N-terminal 10aa)-6xHis or its mutant W_6AW_9A-6xHis to evaluate direct and specific binding, followed by IB with αGST (right). See also Figure S1.

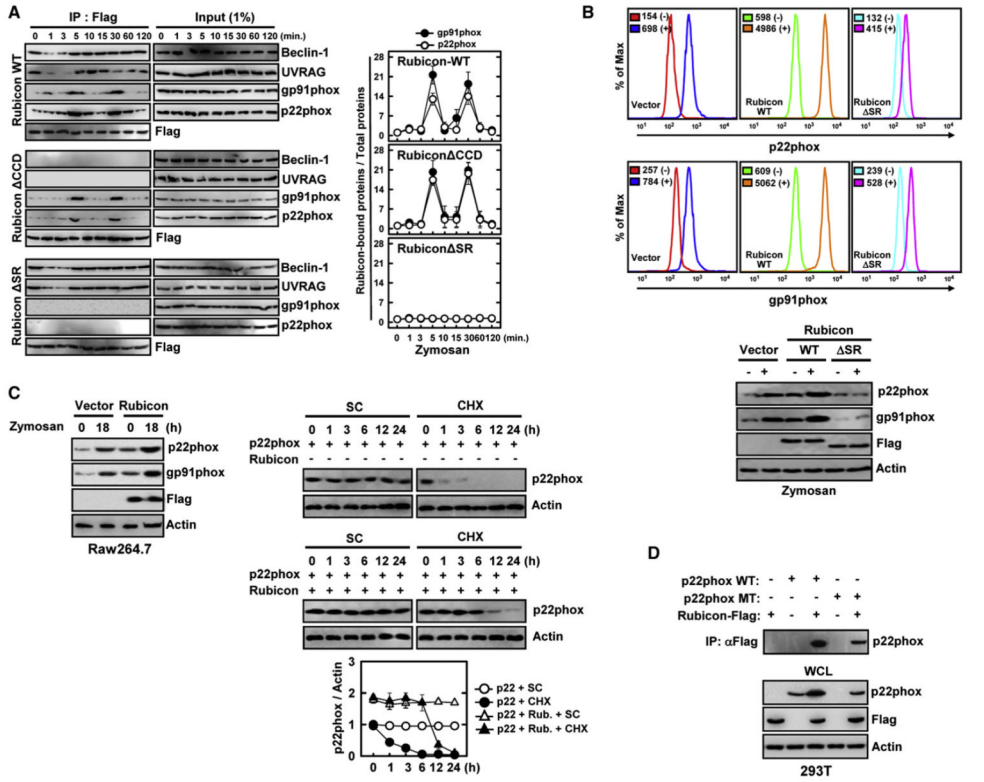

Figure 2. Rubicon Interaction Leads to p22*phox*-gp91*phox* Stabilization

(A) Differential Rubicon interactions. Raw264.7 cells containing vector, Flag-Rubicon WT or its mutant were stimulated with zymosan for the indicated times, followed by IP with αFlag and IB with αBeclin-1, αUVRAG, αgp91*phox*, αp22*phox* or αFlag. The right panels show the densitometry results of all three independent coIP assays.

(B) (top) Rubicon-mediated increases of p22*phox* and gp91*phox* levels. THP-1 cells containing vector, Rubicon WTor ΔSR were stimulated with (−) or without zymosan (+) for 18 hr and used for flow cytometry analysis to detect intracellular p22*phox* or surface expressing gp91*phox*. (bottom) IB with αp22phox, αgp91phox, αflag and αActin.

(C) Rubicon-mediated increases of p22*phox* and gp91*phox* stability. (left) Raw264.7 cells containing vector or Flag-Rubicon were stimulated with zymosan for 18 hr, followed by IB with αp22phox, αgp91phox, αflag and αActin. (right) At 24 hr post-transfection with p22*phox* and/or Flag-Rubicon, 293T cells were treated with solvent control (SC) or cyclohexamide (CHX, 1 μg/ml) for indicated times and cell lysates were used for IB with αp22phox and αActin. The bottom panel shows the ratio of p22*phox*/Actin during CHX time course treatment.

(D) Analysis of p22phoxY_{121}H mutant expression upon Rubicon expression. At 48 hr post-transfection with Flag-Rubicon and/or p22*phox* WTor Y_{121}H mutant, 293T cell lysates were used for IP with αFlag and IB with αp22*phox*. WCLs were used for IB with αp22*phox*, αFlag, or αActin. See also Figure S2.

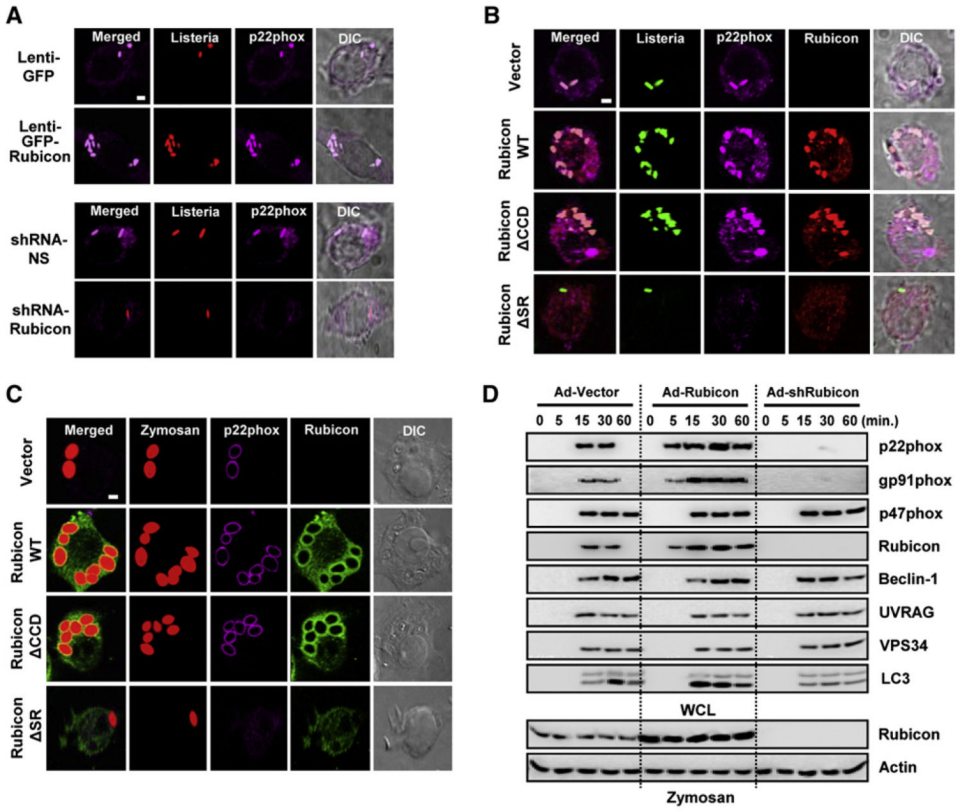

Figure 3. Rubicon Affects p22*phox*Phagosome Recruitment and Phagocytosis

(A–C) (A) Expression or depletion of Rubicon affects the colocalization of p22*phox* with *L. monocytogenes*-containing phagosomes. At 48 hr postinfection with lenti-GFP or lenti-GFP-Rubicon (top) at MOI =100 (Figure S3A) or with lenti-shRNA-NS or lenti-shRNA-Rubicon (bottom) at MOI =50 (Figure S3B), Raw264.7 cells were infected with HK-TRITC-labeled L. monocytogenes (MOI = 1) for 30 min, followed by confocal microscopy with αp22*phox*. Bar, 2 μm. Rubicon enhances the colocalization of p22*phox* with *L. monocytogenes* (B) or zymosan particles-containing phagosomes (C) in a p22*phox*-binding-dependent manner. Raw264.7 cells containing vector, Rubicon WT, ΔCCD or ΔSR were infected with HK-GFP-*L. monocytogenes* (B) or Texas red-labeled opsonized-zymosan particles (C) for 30 min, followed confocal microscopy with αp22phox or αFlag. Bar, 2 μm.

(D) Rubicon enhances phagocytosis in a p22*phox*-binding-dependent manner. At 48 hr postinfection with recombinant Ad-Vector (MOI = 200), Ad-Rubicon (MOI = 100), or Ad-shRubicon (MOI = 200) virus, Raw264.7 cells were stimulated with zymosan-coated particles for indicated times, followed by lysis and sucrose-gradient ultracentrifugation to isolate the bead-containing phagosomal fractions. Phagosomal fractions were subjected to IB with αBeclin-1, αUVRAG, αgp91*phox*, αp22*phox*, αp47*phox*, αVPS34, αLC3 or αRubicon. WCL were used for IB with αRubicon or αActin. See also Figure S3.

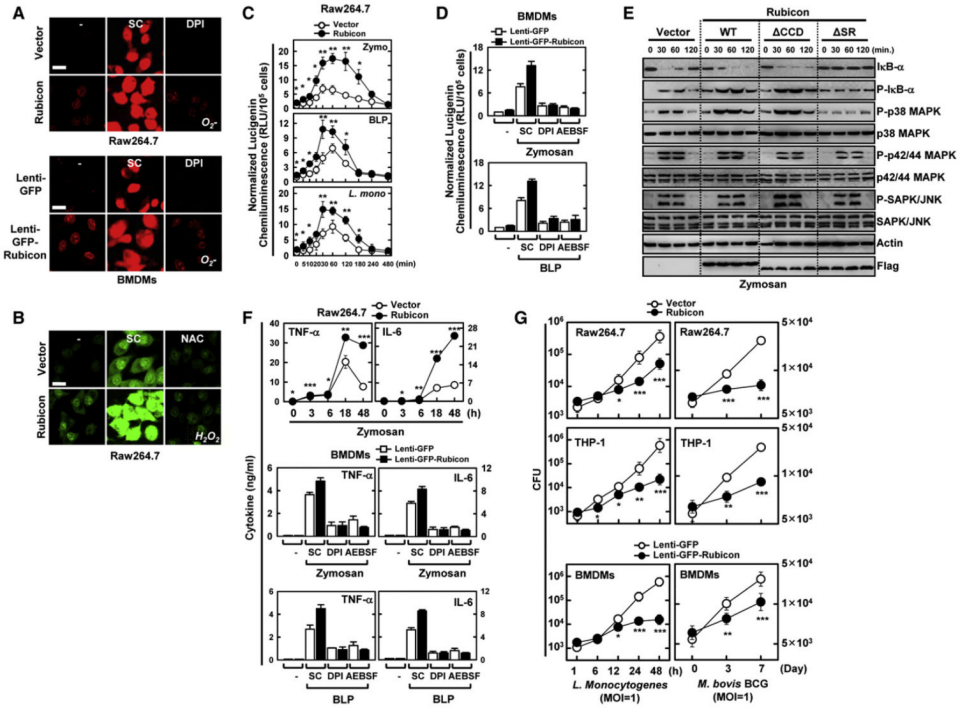

Figure 4. Rubicon Activates NADPH Oxidase Activity in a p22*phox*-Binding-Dependent Manner

(A and B) Rubicon activates ROS production. Raw264.7 cells or BMDMs were incubated with 20 μM DPI (A) and 20 mM NAC (B) to detect O_2^- and H_2O_2 production, respectively, with or without zymosan for 30 min. Live cells were washed with serum-free medium and imaged using a confocal microscope. Bar, 10 μm.

(C) Luminometry of NADPH oxidase activity of Raw264.7 cells containing vector or Rubicon after treatment with zymosan or BLP, or infected with *L. monocytogenes* (MOI = 1).

(D) Rubicon enhances NADPH oxidase activity. BMDMs infected with lenti-GFP or lenti-GFP-Rubicon was analyzed for NADPH oxidase activity upon zymosan or BLP treatment.

(E) Rubicon expression enhances downstream signaling. Raw264.7 cells containing vector, Rubicon or its mutants were stimulated with zymosan for the indicated times and then subjected to IB with the phosphorylated and total forms of p38, p42/p44 MAPK, JNK, IκB-α, or Actin.

(F) Increase of cytokine production by Rubicon. (top) Raw264.7 cells containing vector or Rubicon were stimulated with zymosan for the indicated times and the supernatants were analyzed for cytokine ELISA. (middle and bottom) BMDMs infected with lenti-GFP or lenti-GFP-Rubicon were stimulated with zymosan or BLP for 18 hr and the supernatants were subjected to cytokine ELISA.

(G) Rubicon enhances bacterial killing activity. Raw246.7, THP-1 or BMDMs containing vector or Rubicon were infected with *L. monocytogenes* (left) or *M. bovis* BCG (right) at a MOI = 1 for the indicated times and then lysed to determine intracellular bacterial loads. CFU, colony-forming units. $^{*}p < 0.05$; $^{**}p < 0.01$; $^{***}p < 0.001$ compared with the vector control. All data above are the mean ± SD of values from three experiments. See also Figure S4.

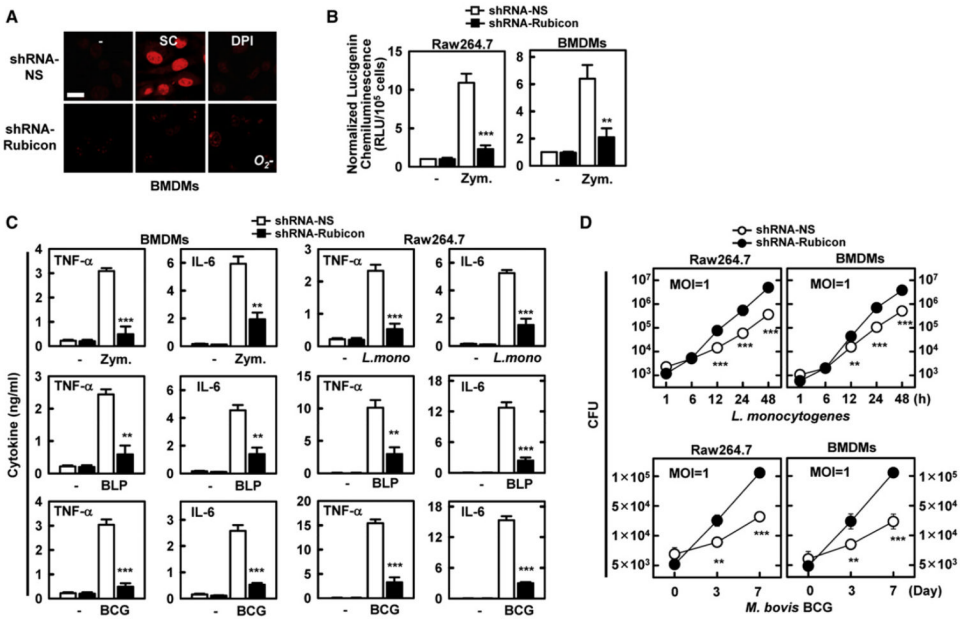

Figure 5. Rubicon's Effect on ROS and Inflammatory Cytokine Production

(A and B) Depletion of Rubicon gene expression leads to the reduction of ROS production (A) and NADPH oxidase activity (B). At 48 hr post-infection with lentivirus-shRNA-NS or lentivirus-shRNA-Rubicon (MOI = 50), Raw264.7 cells or BMDMs were analyzed for O_2^- production upon zymosan treatment for 30 min with or without pretreatment with DPI (A) or for NADPH oxidase activity (B) as described in Figure 4. Bar, 10 μm.

(C) Reduction of cytokine production by Rubicon gene depletion. At 48 hr postinfection with lentivirus-shRNA-NS or lentivirus-shRNA-Rubicon, Raw264.7 cells or BMDMs were stimulated with zymosan, BLP, *L. monocytogenes* or *M. bovis* BCG for 18 hr, and the supernatants were analyzed for cytokine production using ELISA.

(D) Rubicon gene depletion reduces bacterial killing activity. At 48 hr postinfection with lentivirus-shRNA-NS or lentivirus-shRNA-Rubicon, Raw264.7 cells or BMDMs were infected with *L. monocytogenes* (top) or *M. bovis* BCG (bottom) at a MOI = 1 for indicated times and then lysed to determine intracellular bacterial loads. $^{**}p < 0.01$; $^{***}p < 0.001$ compared with the lentivirus-shRNA-NS culture. All data above are the mean ± SD of values from three experiments. See also Figure S5.

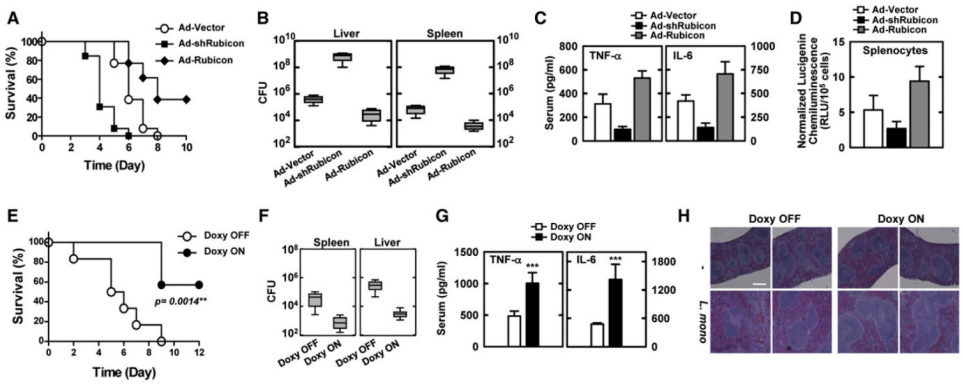

Figure 6. Alteration of Rubicon Gene Expression Affects Mice Mortality after *L.* monocytogenes Infection

(A–D) At 48 hr post-injection with Ad-vector (1×10^{13} pfu/kg), Ad-shRubicon (1×10^{12} pfu/kg),or Ad-Rubicon (1×10^{13} pfu/kg) twice intravenously via the tail vein, mice were infected with L. monocytogenes (1×10^{7} CFU/mouse) and mortality was measured for n = 23 mice per group (A). Bacterial loads of infected mice (n =5 per group) in spleen and liver (B), serum cytokine levels (C) or splenocyte ROS levels (D) were determined at 5 days post-infection with *L. monocytogenes* (1×10^{6} CFU/mouse).

(E–H) Doxycycline-inducible, macrophage-specific expression of Rubicon in SRA-rtTA mice. After 7 days of doxycycline treatment, mice were infected with *L. monocytogenes* (1×10^{7} CFU per mouse) and mortality was measured for n = 6 mice per group (E). *L. monocytogenes* loads of infected mice (n=6 per group) in liver and spleen (F). Serum cytokine levels (G) or H&E staining (I) were determined at 6 days post-infection with *L. monocytogenes* (1×10^{6} CFU/mouse). CFU, colony-forming units. $^{***}p < 0.001$ compared with the doxycycline-off conditions. The data are the mean ± SD of values from three experiments. Bar, 200 μm. See also Figure S6.

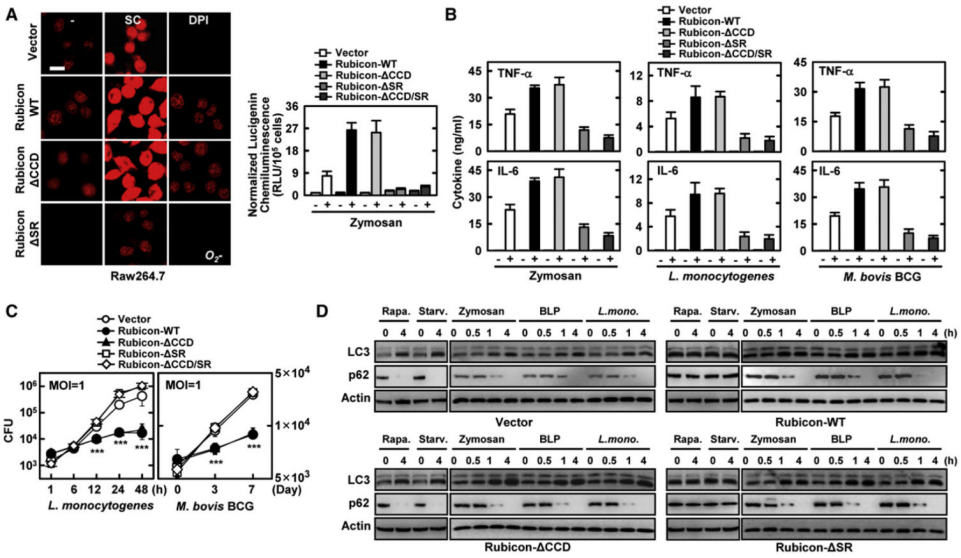

Figure 7. ROS-Mediated Bacterial Killing Activity is p22*phox*-Binding-Dependent

(A) Rubicon enhances ROS production in a p22phox-binding-dependent manner. Raw246.7 cells expressing vector, Rubicon WT, or mutants were used for O_2^- production (left) or for NADPH oxidase activity (right) with or without zymosan for 30 min, as described in Figure 4. Bar, 10 μm.

(B) Rubicon increases cytokine production. Raw264.7 cells containing vector, Rubicon WT or its mutant were stimulated with zymosan, *L. monocytogenes*, or *M. bovis* BCG for 18 h and the supernatants were analyzed for cytokine ELISA.

(C) Rubicon enhances bacterial killing activity. Raw246.7 containing vector, Rubicon WT or its mutant were infected with*L. monocytogenes*(left) or *M. bovis* BCG (right) at a MOI = 1 for the indicated times and then lysed; intracellular bacteria were plated to determine CFU. The data are the mean ± SD of values from three experiments. $^{***}p < 0.001$ compared with the vector control.

(D) Rubicon plays distinctive roles in conventional and TLR-signaling-mediated autophagy. Raw246.7 cells expressing vector, Rubicon WT, ΔCCD, or ΔSR mutant were treated with rapamycin, starvation, zymosan, BLP or *L. monocytogenes* for indicated times and their cell lysates were used forIBwith αLC3, αp62, or αactin. See also Figure S7.